2

International Linear Collider

2.1 Motivations for building linear colliders

The fundamental interactions including electromagnetic, weak and strong interactions between the elementary particles are explained by the Standard Model of particle physics, which has demonstrated huge and continued successes in providing verifiable experimental predictions. However, there remains some unsolved problems in particle physics, which can not be explained by the Standard Model. These problems include:

- **Origin of mass**: the Standard Model postulates a field, called the Higgs field, that gives rise to the asymmetrical force which creates the masses of the quarks, leptons, and bosons. However, it does not explain the properties of this field.

- **Mass hierarchy**: the Standard Model does not explain why the basic particles of matter are the quarks and leptons, or how many of these there should be. In the Standard Model, there is no explanation for the large difference between the masses of the different quarks and leptons. The mass of the top quark is much higher than the one of the others quarks, and this is even more dramatic if we compare to the masses of the leptons. The mass range of all the fermions runs on 11 orders of magnitude, without explanation. Besides, the Standard Model assumed that neutrinos are massless. However, the experimentally established phenomenon of neutrino oscillation requires neutrinos to have nonzero masses [23].

- **Gravity**: gravity as one of the four fundamental forces is not included in the Standard Model, the Standard Model does not explain how gravity is connected to the other forces of nature.

- **Dark matter and dark energy**: the estimated amount of dark matter is ∼27% of the total energy of the universe, much higher than the amount of usual matter, which accounts for only 5% of the total. The rest 68% is given by the dark energy which is thought to be very homogeneous, not very dense and is not known to interact through any of the fundamental forces other than gravity. The Standard Model doesn't contain an explanation for these weakly interacting particles.

- **Matter and antimatter asymmetry**: the Standard Model cannot explain why the universe contains atomic matter made of electrons, protons and neutrons but no comparable amount of antimatter.

Therefore, different theories beyond the Standard Model (also called new physics) are developed to explain these problems. However, in order to find the right theory, experimental validations are essential. These experiments can be divided into three groups: the energy frontier, the intensity frontier and the cosmic frontier (see Fig. 2.1) as described below [24]:

1) The energy frontier: direct production and investigation of new particles using high-energy colliders. These colliders including the currently in use colliders, such as LHC, and future planned colliders, such as ILC, CLIC, CEPC-SppC.

2) The intensity frontier: indirect detection of new phenomenon, using intense particle beams, such at KEKB and BEPC, to uncover properties of neutrinos and observe rare processes that will tell us about new physics beyond the Standard Model. These experiments [25] including the reactor neutrino experiment, such as the MINOS, Double Chooz, Daya Bay [23] and precision measurements of quarks and leptons, such as Mu2e and COMET.

3) The cosmic frontier: direct or indirect detection of new particles (e.g. dark matter) produced in the cosmos using ground and space based detectors. Example of these experiments are AUGER, CDMS and LHAASO.

High-energy colliders, being the energy frontier, have been used to discover new particles and directly probe the architecture of the fundamental forces since the 1960s.

From the view point of colliding particles, there exist two kinds of high-energy colliders: hadron and lepton colliders. Although the hadron colliders (e.g. LHC) are powerful tools to make discoveries by collisions of composite particles (quarks, anti-quarks and gluons), lepton colliders (e.g. ILC) have the advantage of making precision measurements by the collision of "point-like" elementary particles. Beside, leptons do not interact through the strong force, so the background level is lower than with hadron collisions. Therefore, for precision measurements, lepton colliders are preferable.

From the view point of accelerator layout and design, the high-energy colliders can be divided into linear and circular colliders. Comparing with the circular colliders, linear colliders don't suffer from the energy loss by the synchrotron radiation emission [1], which limits the maximum achievable energy of the circular colliders.

Therefore, ILC, being one of the energy frontier machines and being an $e^- - e^+$ linear collider, can provide an ideal setting for detailed exploration of the origin and nature of the Higgs field, dark matter, and other questions of particle physics.

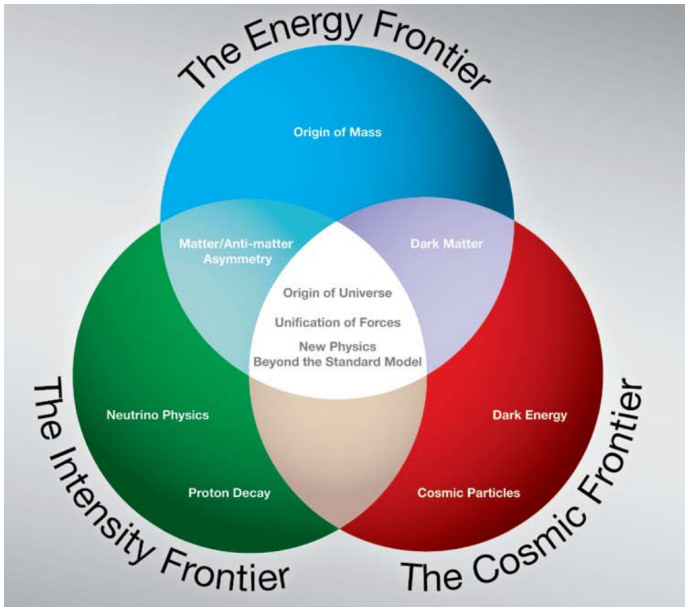

Figure 2.1: Three frontiers of high energy physics with the problems that can be solved by them [24].

[1]The energy loss by synchrotron radiation emission ΔE is proportional to the fourth power of the particle energy E:$\Delta E \propto \frac{E^4}{R}$, where R is the radius of the ring [26].

2.2 Design of the ILC

ILC is a high-luminosity linear electron-positron collider based on 1.3 GHz superconducting radio-frequency (SCRF) accelerating technology. Its centre-of-mass energy range is 200-500 GeV (extendable to 1 TeV), which has been optimised to provide the maximum attainable physics performance with a relatively low risk and minimum cost.

2.2.1 Parameter optimizations for ILC

One of the key requirements the physics community has to the builders of a collider is to reach a certain luminosity. The goals for ILC are particularly challenging, as a luminosity an order of magnitude larger than ever reached in a high energy electron position collider is required [27].

The luminosity of collision is given by [28]:

$$L = \frac{f_{rep} n_b N^2}{4\pi\sigma_x\sigma_y} H_D \tag{2.1}$$

where f_{rep} is the repetition frequency of the bunch trains, N is the number of particles of the colliding bunches, n_b is the number of bunches per train, σ_x and σ_y correspond to the horizontal and vertical beam sizes at the Interaction Point (IP), and H_D is the enhancement factor resulting from self focusing of the beams during the collisions.

From the definition given by Eq. 2.1 it can be seen that for a high luminosity, high f_{rep}, n_b and N are important, as well as, small σ_x and σ_y. To obtain a given luminosity, several constraints and effects must be considered when specifying the parameters [29]:

- The repetition frequency f_{rep} of the trains and the number of bunches per train n_b are defined by the accelerating technology. f_{rep} is also driven by the total power cost.

- The colliding bunch population N is mainly limited by electromagnetic wake-field effects which kick the bunches and can increase their effective size. Wake-fields are generally lower in ILC with its large cavities running at 1.3 GHz than in the Compact Linear Collider (CLIC) with its narrow cavities running at 12 GHz.

- The horizontal beam size is limited by the need to limit the emission of beamstrahlung [1] [30] (see Eq. 2.2 for the beamstrahlung power emission function of the center-of-mass energy E_{cm}) at the level of a few % of the beam energy, while the vertical beam size is limited by the chromaticity correction which depends on the optics design and by the possibility to correct for high order beam aberrations. The beamstrahlung can be expressed as [31]:

$$\delta_B \approx 0.86 \frac{e r_e^3}{2 m_0 c^2} \left(\frac{E_{cm}}{\sigma_z} \right) \frac{N^2}{(\sigma_x + \sigma_y)^2} \tag{2.2}$$

  where e is the electron charge, r_e the classical electron radius, N the number of particles colliding, and $\sigma_{x,y,z}$ the beam sizes in the three spatial dimensions.

- The longitudinal beam size is limited by the hourglass effect [32] if the beam size is long compared to the longitudinal extent of the focal point, it will decrease the luminosity. The vertical beta function at the IP must be similar to the longitudinal beam size or at least it should not be much smaller than σ_z. Bunch compressors can be used to reduce the longitudinal beam size to allow a stronger focusing.

Comparing Eq. 2.1 and Eq. 2.2, it can be seen that it is desirable to make $(\sigma_x \sigma_y)$ small to maximize the luminosity while keeping $(\sigma_x + \sigma_y)$ large to reduce the relative energy loss δ_B. A compromise solution for this is a "flat beam" with $\sigma_x \gg \sigma_y$.

The parameters for several center-of-mass energies including possible upgrades and staging for ILC are shown in Table 2.2. These parameters represent conservative operating points resulting from optimisation subject to the constraints imposed by the various accelerator sub-systems [8].

[1] Beamstrahlung is the synchrotron radiation from a particle being deflected by the collective electromagnetic field of the opposing bunch.

Centre-of-mass energy	E_{CM}	GeV	Baseline 500 GeV Machine				1st Stage	L Upgrade	E_{CM} Upgrade	
			250	350	500		250	500	A 1000	B 1000
Collision rate	f_{rep}	Hz	5	5	5		5	5	4	4
Electron linac rate	f_{linac}	Hz	10	5	5		10	5	4	4
Number of bunches	n_{b}		1312	1312	1312		1312	2625	2450	2450
Bunch population	N	$\times 10^{10}$	2.0	2.0	2.0		2.0	2.0	1.74	1.74
Bunch separation	Δt_{b}	ns	554	554	554		554	366	366	366
Pulse current	I_{beam}	mA	5.8	5.8	5.8		5.8	8.8	7.6	7.6
Main linac average gradient	G_{a}	MV m^{-1}	14.7	21.4	31.5		31.5	31.5	38.2	39.2
Average total beam power	P_{beam}	MW	5.9	7.3	10.5		5.9	21.0	27.2	27.2
Estimated AC power	P_{AC}	MW	122	121	163		129	204	300	300
RMS bunch length	σ_{z}	mm	0.3	0.3	0.3		0.3	0.3	0.250	0.225
Electron RMS energy spread	$\Delta p/p$	%	0.190	0.158	0.124		0.190	0.124	0.083	0.085
Positron RMS energy spread	$\Delta p/p$	%	0.152	0.100	0.070		0.152	0.070	0.043	0.047
Electron polarisation	P_-	%	80	80	80		80	80	80	80
Positron polarisation	P_+	%	30	30	30		30	30	20	20
Horizontal emittance	$\gamma\epsilon_{\mathrm{x}}$	µm	10	10	10		10	10	10	10
Vertical emittance	$\gamma\epsilon_{\mathrm{y}}$	nm	35	35	35		35	35	30	30
IP horizontal beta function	β^*_{x}	mm	13.0	16.0	11.0		13.0	11.0	22.6	11.0
IP vertical beta function	β^*_{y}	mm	0.41	0.34	0.48		0.41	0.48	0.25	0.23
IP RMS horizontal beam size	σ^*_{x}	nm	729.0	683.5	474		729	474	481	335
IP RMS veritcal beam size	σ^*_{y}	nm	7.7	5.9	5.9		7.7	5.9	2.8	2.7
Luminosity	L	$\times 10^{34}$ cm^{-2}s^{-1}	0.75	1.0	1.8		0.75	3.6	3.6	4.9
Fraction of luminosity in top 1%	$L_{0.01}/L$		87.1%	77.4%	58.3%		87.1%	58.3%	59.2%	44.5%
Average energy loss	δ_{BS}		0.97%	1.9%	4.5%		0.97%	4.5%	5.6%	10.5%
Number of pairs per bunch crossing	N_{pairs}	$\times 10^3$	62.4	93.6	139.0		62.4	139.0	200.5	382.6
Total pair energy per bunch crossing	E_{pairs}	TeV	46.5	115.0	344.1		46.5	344.1	1338.0	3441.0

Figure 2.2: Summary table of the 250-500 GeV baseline and luminosity and energy upgrade parameters [8].

2.2.2 Accelerator components

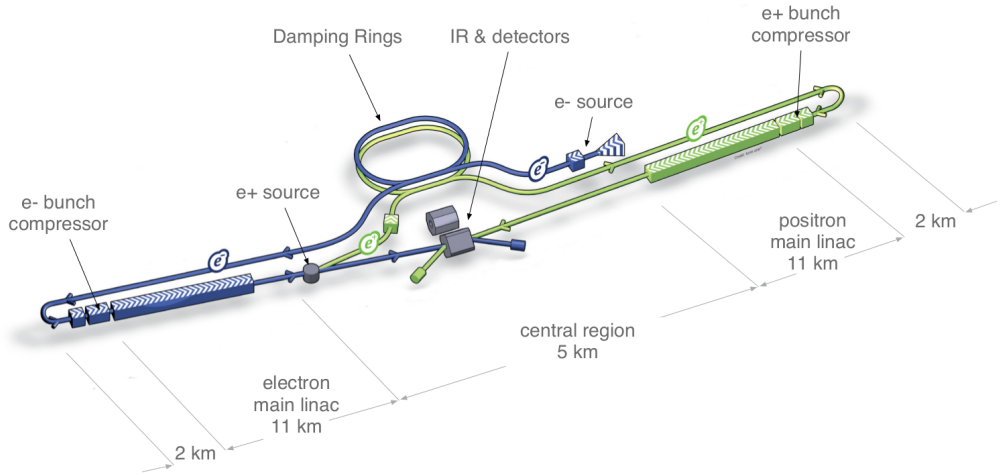

Figure 2.3: Schematic layout of the ILC, indicating all the major subsystems (not to scale) [8].

The ILC accelerator complex consists of polarised electron and positron sources, two damping rings (DR) with a circumference of 3.2 km, two Ring To Main Linac (RTML) transport lines, two 11 km main linacs and two 2.2 km Beam Delivery Systems (BDS) (see Fig. 2.3). The total length of the ILC complex is $\sim$ 31 km long.

Electron source

In a linear collider, polarised beams are preferred as the collision of two polarised beams can suppress some background processes and improve signal to noise ratio thereby enhancing the effective luminosity [33]. Therefore polarised electron and positron sources are essential.

The polarised electron sources are based on a photocathode DC gun. The schematic layout of this system is shown in Fig. 2.4.

The electron beam is produced by a laser illuminating a strained GaAS photocathode in a DC gun, providing the necessary bunch train with greater than 80% polarisation. Two independent laser and gun systems provide redundancy. The produced beam with a bunch charge of 4.5-5 nC and bunch length of 1 ns is bunched down to about 20 ps and pre-accelerated to 76 MeV by normal-conducting structures. After that, a

superconducting linac is used to accelerate the beam up to 5 GeV. Before injection into the damping ring, superconducting solenoids rotate the spin vector into the vertical, and a separate Type A (see Section 2.2.2)superconducting RF cryomodule is used for energy compression.

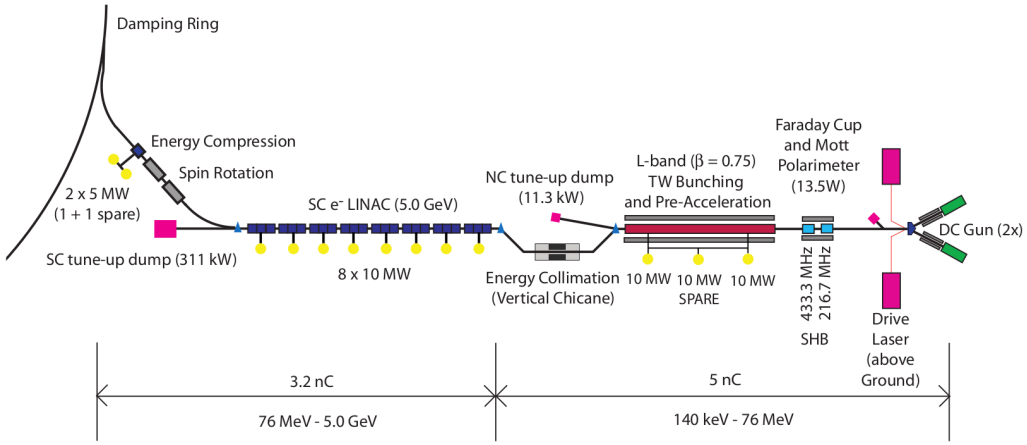

Figure 2.4: Schematic view of the polarised electron source [8].

Positron source

For the polarised positron source, the positrons are obtained from electron-positron pairs by converting high energy photons produced by the up to 150 GeV main electron beam passing through a 147 m superconducting helical undulator. The schematic layout of this system is shown in Fig. 2.5.

To generate photons from undulator radiation, the electron beam for collision is used. The generated polarized photons with maximum energies from $\sim$ 10 MeV up to $\sim$ 30 MeV are directed onto a rotating 0.4 radiation-length Ti-alloy target $\sim$ 500 m downstream, where electron-positron pairs are produced [1]. A normal conduction L-band RF and solenoid focusing system captures the positrons and accelerates them to 125 MeV. The electrons and remaining photons are separated from the positrons and dumped. The positrons are accelerated to 400 MeV in a normal conducting L-band linac with solenoid focusing. After that, the positrons undergo the acceleration, spin

[1]Since a large amount of gamma rays concentrate on the short duration, the production target destruction is feared. To mitigate this effect, a 100 m/s target rotation speed is required [26].

rotation and energy spread compression processes similar to the electrons before the injection to positron damping ring.

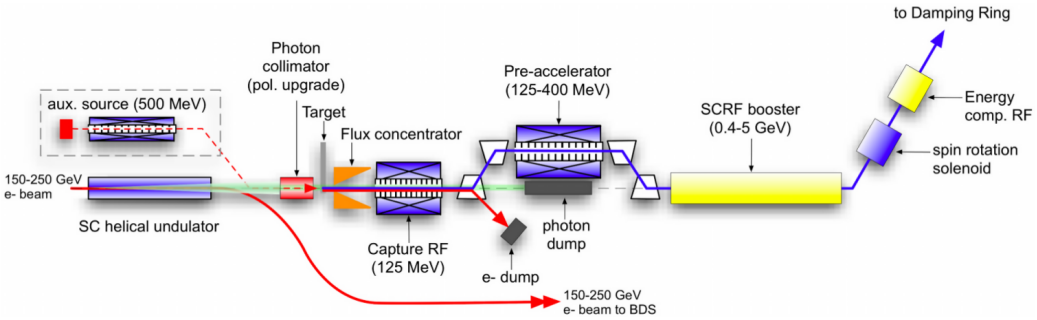

Figure 2.5: Schematic view of positron source [8].

Damping rings

The damping rings must accept e and e^+ beams with large transverse and longitudinal emittances and damp them (by five orders of magnitude for the positron vertical emittance) to the low-emittance beam required for luminosity production, within the 200 ms between machine pulses (100 ms for 10 Hz mode), which is accomplished by approximately 113 m of superferric wigglers (54 units $\times$ 2.1 m) in each damping ring. This technology makes the particles radiate as fast as possible. Besides, the damping ring must compress on injection and decompress on extraction the $\sim$1 ms beam pulse by roughly a factor of 90 to fit into the ring circumference of 3.2 km.

The damping ring lattice follows the race-track design shown schematically in Fig. 2.6. The two arc sections are constructed from 75 Theoretical Minimum Emittance (TME) cells. One of the two 712 m-long straight sections accommodates the RF cavities, damping wigglers, and a variable path length to accommodate changes in phase (phase trombone), while the other contains the injection and extraction systems, and a circumference-adjustment chicane.

The emittance required for linear colliders has already been successfully demonstrated in the ATF damping ring, where a horizontal emittance of 3 μm·rad and a vertical emittance of 30 nm·rad were obtained, much smaller than that achieved by the SLAC Linear Collider (SLC) as shown in Fig. 2.6 (right).

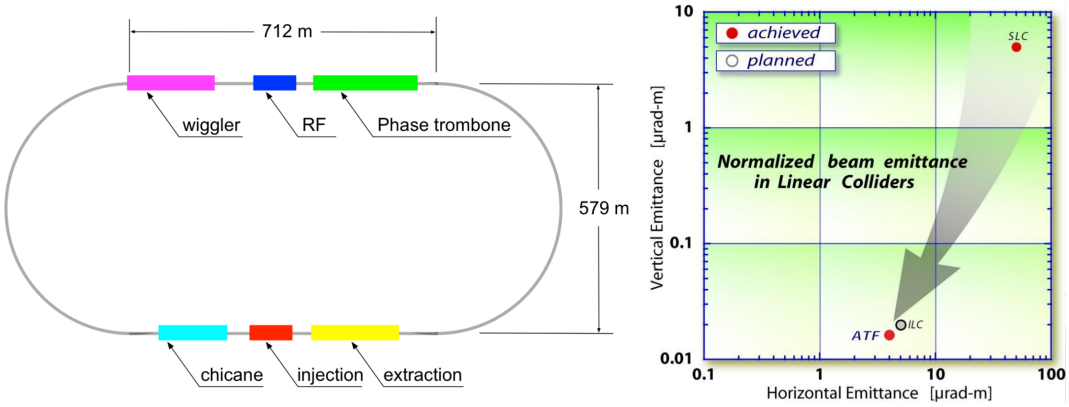

Figure 2.6: Schematic view of the damping ring [8] and the achieved emittance [26].

Ring to main linac

The electron and positron Ring to Main Linac (RTML) systems are the longest contiguous beamlines in the ILC. The layout of the RTML is identical for both electrons and positrons, and is shown in Fig. 2.7. The RTML consists of the following subsystems, representing the various functions that it must perform:

- a 15 km long 5 GeV transport line (ELTL);
- betatron- and energy-collimation systems (in ERTL);
- a 180° turn-around, which enables feed-forward beam stabilisation (ETURN);
- spin rotators to orient the beam polarisation to the desired direction (ESPIN);
- a two-stage bunch compressor to compress the beam bunch length from several millimetres to a few hundred microns, as required at the IP (EBC1 and EBC2).

The two-stage bunch compressor includes acceleration from 5 GeV to 15 GeV in order to limit the increase in fractional energy spread associated with bunch compression. The acceleration is provided by sections of SCRF main-linac technology. A primary challenge for the RTML systems is the preservation of the emittance extracted from the damping rings; the combination of the long uncompressed bunch from the damping ring and large energy spread (after compression) make the tuning and tolerances particular demanding. However, tuning techniques developed from detailed simulations have demonstrated acceptable emittance growth [8].

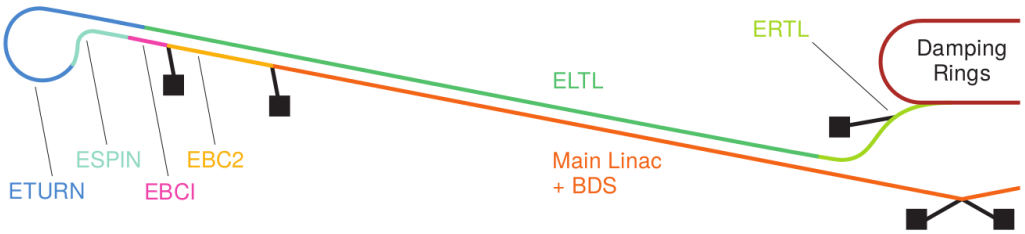

Figure 2.7: Schematic view of the electron RTML system (the positron system is a mirror image [8].

Main Linac

The ILC Main Linacs accelerate the beam from 15 GeV to a maximum energy of 250 GeV with an average accelerating gradient of 31.5 MV/m. Beam acceleration is provided by $\sim$ 7400 1.3 GHz and 1 m long superconducting nine-cell niobium cavities operating at 2 K, assembled into $\sim$ 850 cryomodules (see Fig. 2.8). Each crymodule is 12.65 m long and there are two types: Type A with nine 1.3 GHz nine-cell cavities and Type B with eight nine-cell cavities and one superconducting quadrupole package located at the center of the module.

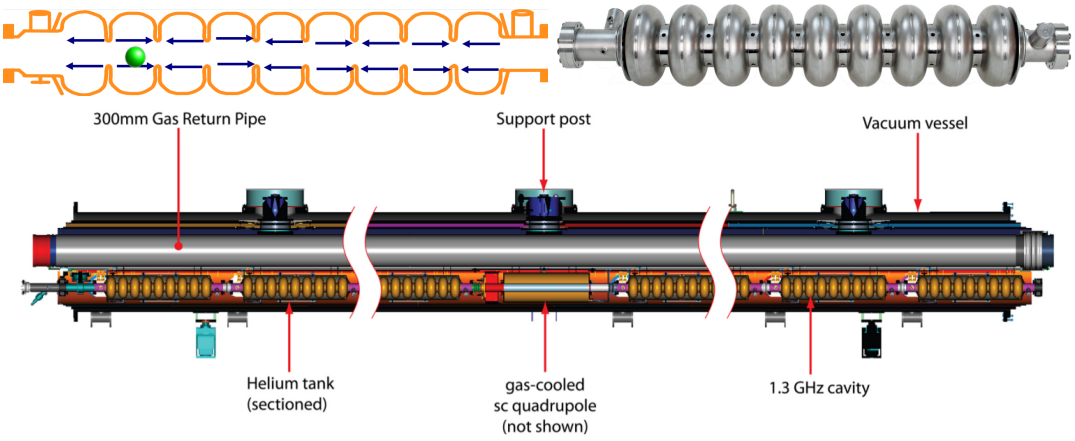

Figure 2.8: A 1.3 GHz superconducting niobium nine-cell cavity with its schematic layout (upper) and longitudinal cross section of the ILC cryomodule (Type B) (lower) [8].

Beam Delivery System

The BDS is responsible for transporting the beams from the exit of the high energy linacs, focusing them to the required sizes, bringing them into collision, and transporting the spent beams to the main beam dumps. The layout of BDS is shown in Fig. 2.9. It consists of five main subsystems:

- **Diagnostic**: this section contains emittance measurement and matching (correction), trajectory feedback, polarimetry and energy diagnostics;
- **The collimation system**: the collimation system removes beam-halo particles that would otherwise generate unacceptable background in the detector and also contains magnetised iron shielding to deflect muons generated in the collimation process;
- **The final focus system (FFS)**: the FFS uses strong compact superconducting quadrupoles to focus the beam at the IP, with sextupoles providing local chromaticity correction;
- **The interaction region**: the interaction region can be occupied by two detectors in a so-called "push-pull" configuration;
- **The extraction line**: the extraction line has a large-enough bandwidth to cleanly transport the heavily disrupted beam to a high-power water-cooled dump, and also contains important polarisation and energy diagnostics.

The collimation system and the FFS are described in more detail in the following sections.

2.2.3 Beam halo and beam halo collimation in linear colliders

One of the main challenges of the BDS design for the linear collider is to remove the large amplitude particles (beam halo) from the linac to minimize background in the detectors [34].

In linear accelerators, the sources of beam halo formation can be divided into three groups [35]:

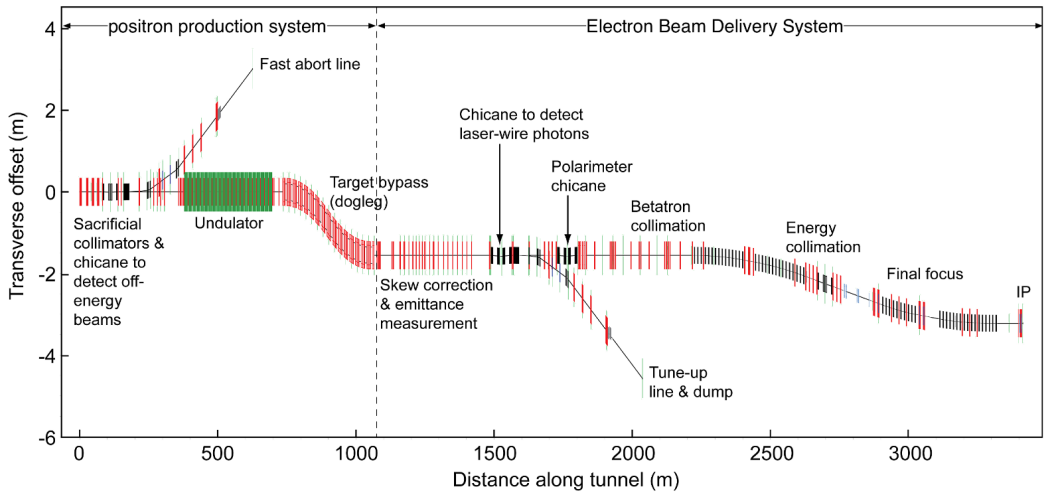

Figure 2.9: BDS lattice layout, showing the major sub-systems. Shown is the electron BDS, which starts at the vertical dotted line. (Also shown is the positron system upstream of the electron BDS). The positron BDS is a mirror image.

- **particle process sources**: beam gas scattering, intra-beam scattering, (quasi) elastic and inelastic bremsstrahlung etc.
- **optical related sources**: mismatch, coupling, dispersion, non-linearities
- **other sources**: regeneration of particles when halo is intercepted, noise and vibration, dark currents, wake-fields, etc.

Interactions of the beam halo with the detector and other components in the BDS would create fluxes of muons and other secondaries which could exceed the tolerable levels at a detector by a few orders of magnitude [14]. Minimisation of detector background needs efficient removal of the beam halo. A collimation system is designed to scrape the beam halo away. The requirements of collimation system is defined by the IR layout [36, 37].

The collimators need to be placed far from the interaction point to minimise the background in the vertex detector (VX). Meanwhile, the beam halo must be collimated upstream in such a way that no beam halo and synchrotron radiation (SR) photons emitted from halo particles reach the final doublet magnets (FD) or the VX. The VX aperture needs to be larger than the FD aperture, and the exit aperture should be larger than the VX aperture.

The beam convergence depends on the optical parameters, while the maximum allowed halo convergence is determined by the geometry, in terms of the maximum allowed amplitude of particles at the entrance of the FD. The ratio $\theta_{halo_{max}}/\theta_{beam}$, defined as the collimation depth, becomes tighter with larger l^* or smaller IP beam size (see Fig. 2.10). A tighter collimation system may lead to problems for the machine protection system (MPS) and induce collimation wake-fields or higher muon flux from collimators [38]. The collimation depths for the ILC design are approximately 8-10 σ_x* and 60-80 σ_y* for the horizontal and vertical planes, respectively.

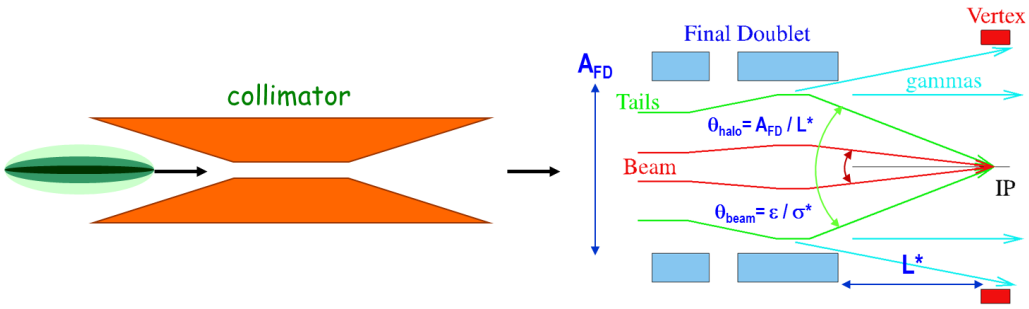

Figure 2.10: Sketch of ILC collimation system (modified from [38]).

The collimation system in the BDS can be divided into two subsystems: upstream and downstream collimation. The upstream collimators are mainly used for betatron and energy collimation and the downstream collimators in the extraction lines [1] serve to protect the magnets from radiation loads [36].

The betatron collimators use a two stage collimation approach: a thin (0.5-1 radiation length) spoiler followed by a thick (20 radiation length) absorber at the appropriate phase advance in the lattice [34]. This two stage design can mitigate the collimator damage due to the intense beam.

The energy collimators help to remove the degraded energy particles originating from the betatron collimation section but not absorbed there. The energy collimation section has a single spoiler located at the central high dispersion point.

Fig. 2.11 shows the optics of the BDS, starting from the entrance of the collimation system to the IP. The location of the spoilers and absorbers are shown. The collimators are placed both at FD betatron phase and at IP phase with two spoilers per FD and IP phase. The energy collimator is placed in the region with large dispersion and

[1] The extraction line guide the beam and the bremsstrahlung from the IR to the beam dumps.

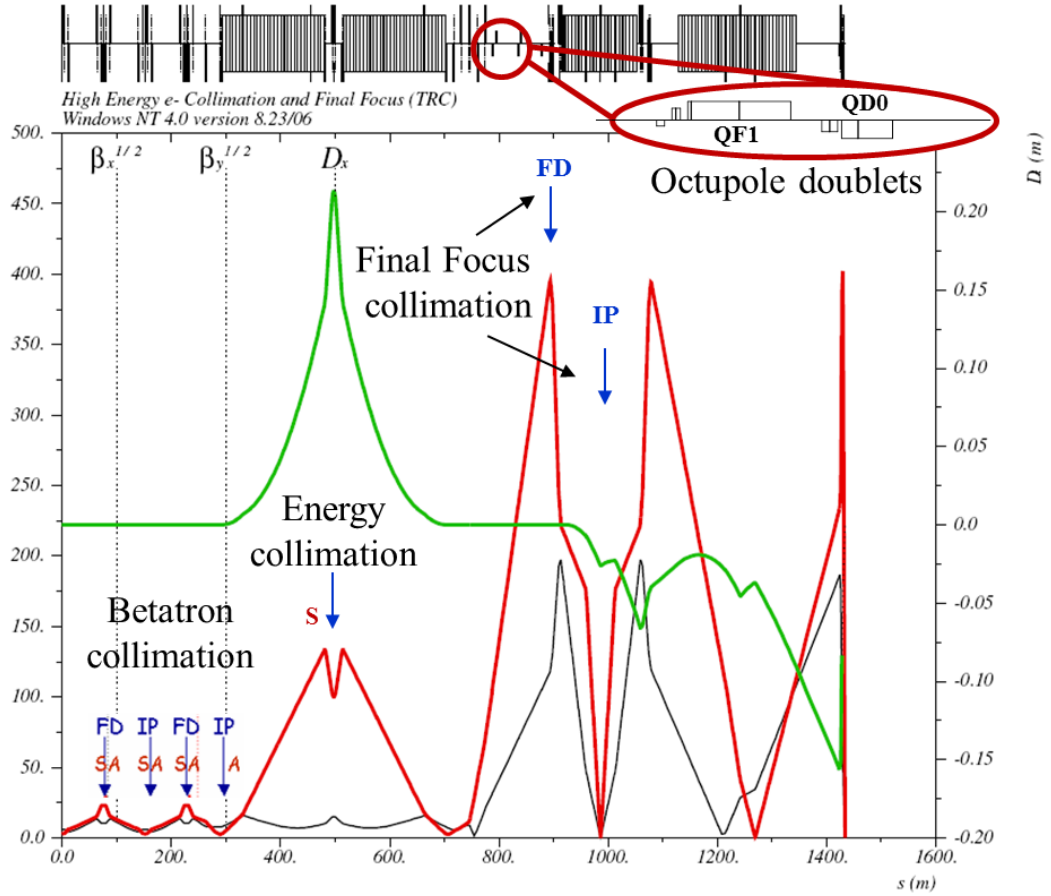

Figure 2.11: An earlier version of BDS optics (from the entrance of collimation system to the IP), with consumable spoilers (S) and absorbers (A) (modified from [37, 34]).

secondary clean-up collimators are located in the final focus system (FFS). Beside, the FFS includes two superconducting octupole doublets which use nonlinear focusing to reduce the amplitudes of beam halo particles while leaving the beam core untouched [37]. This tail-folding would permit larger collimation amplitudes, which in turn would reduce the amount of beam power intercepted and the unwanted wakefields [39].

2.3 Final Focus System

The FFS utilises a number of quadrupoles (minimum 4) to construct a telescope to "demagnify" the incoming beam ellipse to a smaller size. The schematic layout of the telescope optics for the FFS is shown in Fig. 2.12. In this optics, two final lenses (final

doublet (FD)) are used before the IP for the final focus, one mainly for x and another mainly for y. Use this optics, the beam size can be demagnified by a factor:

$$m = f_1/f_2 = f_1/l^* \tag{2.3}$$

where f_1 and f_2 are the focal lengths of the first two lenses and the FD respectively, and $l^* = f_2$ represents the distance between the FD and the IP. The focal lengths are defined by the magnet strengths. For the ILC, the design value of l^* is about 4 m [1]. Very strong superconducting quadrupoles with gradients of the order of hundreds of Tesla per meter are required to reach focal lengths of this order.

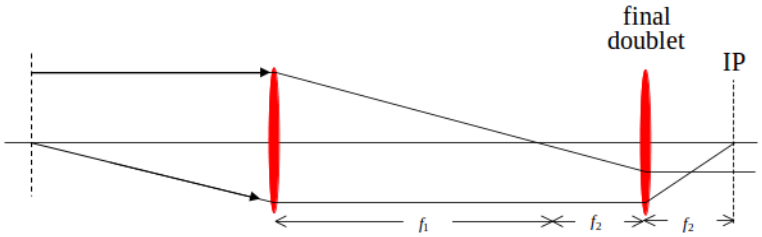

Figure 2.12: Telescope optics for the FFS.

2.3.1 Chromaticity aberration

If there would be no energy spread in the beam, a telescope optics could serve as the FFS. However, the electron beam with a certain energy spread (σ_E) passing through a focusing magnet can get dispersed and distorted, this effect is called chromatic aberration. Since the on-momentum ($p = p_0$) and off-momentum ($p < p_0$ or $p > p_0$) particles experience different kicks from the magnetic field, the beam size at the interaction point (IP) is enlarged (see Fig. 2.13). The particle displacement at the IP is given by [40]:

$$\Delta y^* \approx l^* \delta\theta \tag{2.4}$$

where l^* is the distance from FD to the IP, $\delta = (E - E_0)/E_0$ is the relative energy deviation with respect to the reference particle and θ is the angluar spread.

Assuming there is no initial correlation between energy and angle, the RMS vertical beam size (σ_y) at the IP can be expressed as:

$$\Delta\sigma_y^* = l^*\sigma_\theta^*\sigma_E = l^*\sqrt{\frac{\epsilon}{\beta^*}}\sigma_E \tag{2.5}$$

[1] 3.5 m for SiD detector and 4.5 m for ILD detector.

where $\sigma_\theta^* = \sqrt{\frac{\epsilon}{\beta^*}}$ is the nominal vertical angle at the IP and σ_E is RMS value of energy deviation (δ). Then the chromatic dilution of the beam size can be obtained as:

$$\frac{\Delta\sigma_y^*}{\sigma_y^*} = l^* \sqrt{\frac{\epsilon}{\beta}} \frac{1}{\sqrt{\epsilon\beta^*}} \sigma_E = W\sigma_E \quad with \quad W = \frac{l^*}{\beta^*} \tag{2.6}$$

where $\sigma_y^* = \sqrt{\epsilon\beta^*}$ is the nominal beam size and W is defined as the chromaticity, which is determined by l^*, i.e. the focal strength of the FD, and β^*, i.e. the depth of focus of optical image at the IP. For the ILC design with the SiD detector, where $l^* = 3.5$ m, $\beta^* \approx 0.4$ mm and $\sigma_E \approx 0.1\%$, the chromaticity dilution $\Delta\sigma_y^*/\sigma_y^* \approx 9$, which means that the chromatic aberration would completely dominate the IP vertical beam size, hence it is essential to correct it.

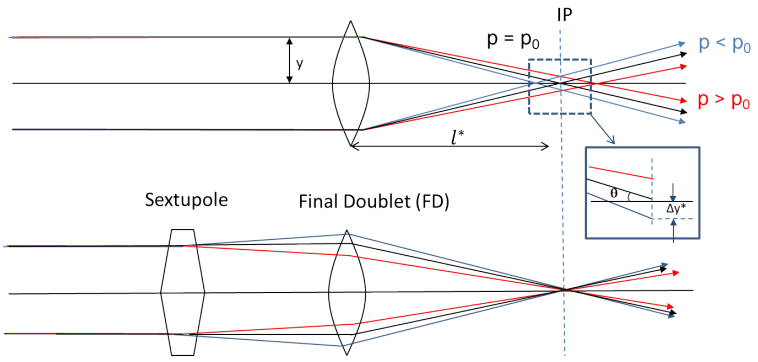

Figure 2.13: Chromaticity aberration from the strong final doublet for a particle with on and off-momentum respect to the nominal value (upper) and the correction of it by a sextupole magnet (lower) (modified from [41]).

2.3.2 Chromaticity Correction

The chromaticity correction can be done by adding sextupoles located in the region with horizontal dispersion upstream of the FD, because the focal strength of the sextupoles is proportional to the particle energy (see Fig. 2.13 (lower)) [41]. Two different conceptual designs of chromaticity correction have been developed over the last decades, which are refered to as non-local [42] and local [43] chromaticity corrections.

Non-local Chromaticity Correction

The "traditional" (non-local) chromaticity correction design utilised two pairs of -I separated sextupoles, for x and y chromaticity compensation (see Fig. 2.14 (upper)).

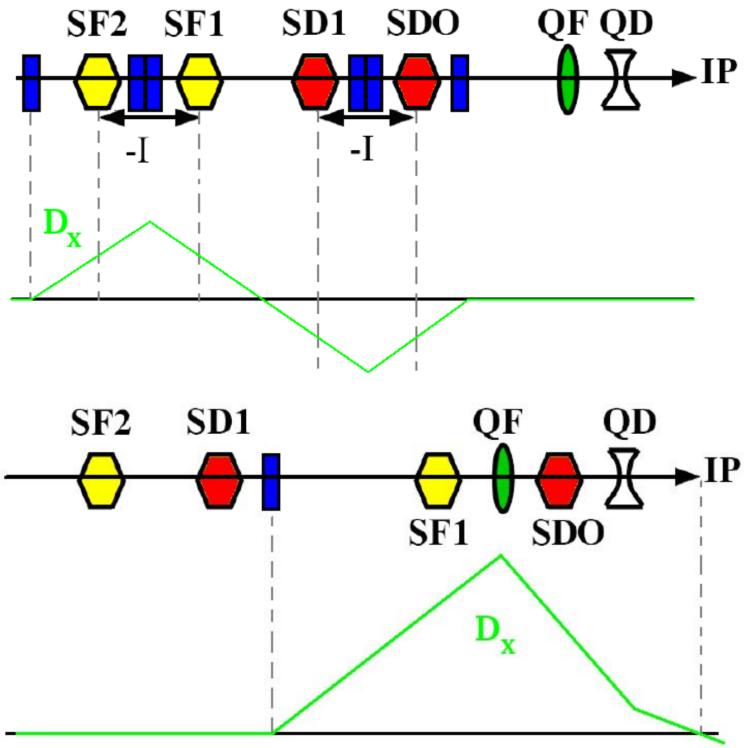

Figure 2.14: Non-local (upper) and local (lower) chromaticity correction.

The two pairs were typically non-interlaced, to minimise the third and higher order aberrations. All earlier designs followed this principle including the SLC and FFTB optics [44], which were both realised experimentally. However, this way of correcting the chromaticity has several limitations due to the fact that the chromaticity is created in the FD near IP, but is pre-compensated 1000 m upstream as the bend magnets and the collimation sections have to be sufficiently long in this design [45]. Therefore, any disturbances to the beam for example the synchrotron radiation generated energy spread, created between the sextupoles and IP, would disturb the compensation of the chromaticity. Compensation of sextupole aberrations in such a system is also not ideal as $M \neq -I$ for off-energy particles. This in particular creates large aberrations for off-energy particles and especially for the beam tails.

Local Chromaticity Correction

In order to mitigate the problems arising from the non-local chromaticity correction, a novel final focus system with local chromaticity correction was proposed [43]. The idea of this design is to correct the chromaticity as locally as possible, minimize the number of bend magnets, preserve the linear optics as much as possible and to have as few elements as possible. Here below the way of approaching this design is shown analytically.

The horizontal and vertical kick (x' and y') received by a particle with energy deviation of δ from a quadrupole of strength K_Q can be written as:

$$x' \approx (K_Q x - K_Q \delta x) = K_Q(x_\beta + D_x\delta) - K_Q x_\beta \delta - K_Q D_x \delta^2 \tag{2.7}$$

$$y' \approx -(K_Q y - K_Q \delta y) = -(K_Q y_\beta - K_Q \delta y_\beta) \tag{2.8}$$

where $x = x_\beta + D_x\delta$ and y=y_β. The first term in this equation corresponds to the focusing of the beam, the second is the chromaticity term and the third one is the second order dispersion term.

In order to correct the chromaticity term, a focusing sextupole with strength of K_S can be added next to the quadruple. The horizontal kick given by this sextupole can be written as:

$$x^{'} = \frac{1}{2}K_S(x^2 - y^2) = K_S\left[\frac{1}{2}(x_\beta^2 - y_\beta^2) + x_\beta D_x\delta + \frac{1}{2}D_x^2\delta^2\right] \tag{2.9}$$

$$y^{'} = -K_s xy = -K_s(D_x\delta y_\beta + x_\beta y_\beta) \tag{2.10}$$

Here the first term corresponds to the geometric aberration, the second one is the chromaticity and the last one is the second order dispersion.

Comparing Eq. 2.7 with Eq. 2.9 and Eq. 2.8 with Eq. 2.10, it can be seen that by setting $K_S = K_Q/D_x$ the term with δ can be cancelled directly in y, however, in x only the chromaticity term can be cancelled completely, the second order dispersion term is only cancelled by half. The geometric terms still need to be cancelled in both x and y.

For the second order term cancellation, a second focal point is introduced in a non dispersive region (see Fig. 2.11) doubling the overall chromaticity and hence the sextupole strengths required to correct it. The geometric term is cancelled in the same way as in the non-local chromaticity correction design by adding another pair of

sextupoles upstream in a non-dispersive region at the same phase as the ones in the FD with a -I transformation between the two sextupoles (see Fig. 2.14 (lower)).

To summarise, in the local chromaticity correction design, the chromaticity is cancelled locally by two sextupoles interleaved with the FD, a bend upstream is needed to generate dispersion across the FD needed for sextupoles to work. Besides, the second order dispersion produced by sextupoles in the FD is cancelled locally provided that half of horizontal chromaticity arrives from upstream of FD. Furthermore, the geometric aberrations of the FD sextupoles are cancelled by two more sextupoles placed in phase with them and upstream of the bend. In addition, other higher order aberrations are cancelled by optimising the transport matrices between the sextupoles [45].

Comparing with the non-local chromaticity corrections, the local chromaticity corrections is much shorter and therefore less costly. Meanwhile, it is less sensitive to the beam energy variation and to the fields errors as the non linear terms introduced by the sextupoles are transported on a much shorter distance. Furthermore, it has much less aberrations and it does not mix betatron phases of non-core particles, which is in particular important for minimisation of generation of beam tails and ensuring good performance of the collimation system [45].

Despite these advantages, the complicated design and difficulties in beam tuning during the operation may make it difficult to realise the local chromaticity correction concept, hence it is of great importance to verify it experimentally. The ATF2 final focus, a prototype of a FF with local chromaticity compensation, was therefore designed for this purpose.